A new speckle filtering method for ultrasound images based on a weighted multiplicative total variation

Meriem Hacini, Fella Hachouf, Khalifa Djemal

A new speckle filtering method for ultrasound images based on a weighted multiplicative total variation

Meriem Hacini [a,*], Fella Hachouf [a], Khalifa Djemal [b]

[a] *Laboratoire d' Automatique et de Robotique, Département d' Électronique, Faculté des sciences de l'ingérineur, Université Constantine 1, Route d' Ain el bey, 25000 Constantine, Algeria*
[b] *IBISC Laboratory, University Evry val Essonnes, 40 Pelvoux Street, 91080 EVRY Courcouronnes Cedex, France*

Ultrasound images are corrupted by a multiplicative noise – the speckle – which makes hard high level image analysis. In order to solve the difficulty of designing a filter for an effective speckle removing, we propose a new approach for de-noising images while preserving important features. This method combines a data misfit function based on Loupas et al. model and a Weighted Total Variation (WTV) function as a multiplicative factor in the cost functional. The de-noising process is performed using a multiplicative regularization method through an adaptive window whose shapes, sizes and orienta-tions vary with the image structure. Instead of performing the smoothing uniformly, the process is achieved in preferred orientations, more in homogeneous areas than in detailed ones to preserve region boundaries while reducing speckle noise within regions. Quantitative results on synthetic and real images have demonstrated the efficiency and the robustness of the proposed method compared to well-established and state-of-the-art methods. The speckle is removed while edges and structural details of the image are preserved.

1. Introduction

Ultrasound (US) is a widely used, safe medical diagnostic technique, due to its noninvasive nature, low cost, capability of forming real time imaging and the continuing improvements in image quality [1]. However, the main weakness of medical ultrasound image is the poor quality which interferes with multiplicative speckle noise that degrades the visual evaluation. This phenomenon is common to laser, sonar and synthetic aperture radar (SAR) imagery [2,3]. Speckle pattern is a form of a multiplicative noise. It depends on the structure of imaged tissue and various imaging parameters. Speckle has a negative impact on medical US images. It tends to reduce the image contrast to make obscure and blur image details which affect the human ability to identify normal and pathological tissue. It also degrades the speed and accuracy of ultrasound image processing tasks such as segmentation and registration. The macroscopic properties of studied biological tissues demonstrate that speckle noise tends to mask important details, consequently confusing the diagnosis. The speckle noise is a random process. It does not provide enough information which lead to a wide subject of investigations [2,4–11]. In order to improve the quality of US images, it is imperative to reduce this speckle without destroying the image features. Recently, it has been demonstrated that Total Variation (TV) methods are relevant models for de-noising images in different cases [12–16]. Accordingly, in this paper a variational model to deal with speckle noise in real ultrasound images is proposed. To eliminate the choice of the artificial

* Corresponding author.
E-mail addresses: meriem.hacini@yahoo.fr (M. Hacini), hachouf.fella@gmail.com (F. Hachouf), djemal@iup.univ-evry.fr (K. Djemal).

regularization parameter, the energy functional is chosen as the product of a data fidelity term and a TV regularization term. The multiplicative TV regularization was proposed by van den Berg et al. [17] to solve contrast source inversion problem. In this work, we propose an adaptation of the multiplicative regularization to a dedicated US noise model [11] using a locally adaptive energy minimization based on weighted total variation model. To de-noise US images, the challenge is to enhance and preserve important features; the proposed method is applied on a locally adaptive window, where shapes, sizes and orientations varying with image structures [18]. This proposed Adaptive Weighted Multiplicative Total Variation Regularization method is denoted as AWMTVR.

This paper is organized as follows: in Section 2, we give an overview of speckle filters and related methods. Section 3 describes our adaptive weighted multiplicative Total Variation Filter. Quantitative results on artificial and real US images are presented in Section 4; Section 5 concludes our contribution and describes the future works.

2. Speckle filtering: related works

The need for image processing methods to suppress speckle noise has been proven to enhance image quality and increase diagnostics potential for medical ultrasound images. Therefore image de-noising problem has been studied widely. A number of locally adaptive statistic filters based on multiplicative speckle noise were developed. The typical filtering methods include Lee filter [19], Kuan filter [20], Frost filter [21], enhanced Lee filter and enhanced Frost filter [22]. These filters reduce the speckle noise by adjusting the size of the filtering window. They also decrease the image resolution inside this latter, which makes image edges and linear targets blurry. Some edge information is saved well, but speckle is not fully smoothed. Recently, inverse problems such as image restoration appeared in many applications like remote sensing, medical imaging, astronomy and digital photography [23]. Most of inverse problems are nonlinear and highly ill-posed. In order to solve this problem, a large number of techniques have been developed. One of the most well-known techniques is the Total Variation minimization and regularization. Total variation (TV) is a powerful concept for robust estimation [24]. It was first introduced for regularization in image restoration [25]. It has been extensively used with great success for inverse problems, because the TV has the ability of smoothing noise in flat image areas and at the same time preserves finer image details such as edges and texture, due to the piecewise smooth regularization property of the TV norm. It received many theoretical research attention. It has been used in many signal and image processing applications [16,26–32]. Nevertheless, TV- based image restoration has some drawbacks. One of them is the regularization parameter selection. For this purpose, numerous studies were conducted [33–38]. A solution is to use the multiplicative type of regularization of inverse algorithms, eliminating the choice of the artificial regularization parameters [17]. However, most of existing multiplicative regularization is applied on electromagnetic problems [39–45]. To our knowledge, multiplicative regularization approach has not been applied for speckle reduction in US images. In this aim, we implement the multiplicative regularization within the framework of speckled image de-noising. We combine the data misfit function based on the Loupas et al. noise model [11] and a weighted total variation function as a multiplicative factor in the cost functional. The computation of the appropriate parameter is controlled by the minimization process itself. The minimization is achieved through local adaptive windows. Experiments have proven the excellent performance of the proposed method which constitutes a robust approach for speckled images.

3. Proposed method

Several multiplicative regularization techniques have been developed in different fields, but there are none specific to speckle suppression. Therefore, a new Speckle reduction technique – an Adaptive Weighted Multiplicative Total Variation Regularization method, AWMTVR method – is instituted to reduce the speckle. We first determine the noise model used for US images with a new formulation of the proposed method.

3.1. Notations

The notations below are used.

$d(x,y)$	observed noisy image
$\overline{d}(x,y)$	mean image
$f(x,y)$	original image
$\hat{f}(x,y)$	approximative solution
$b(x,y)$	zero-mean Gaussian noise
$J_{TV}(f,\Omega)$	weighted total variation function
$W(f)$	weight function
$J_R(f,\Omega)$	regularization function
$J(d,f,\Omega)$	cost function
η_R	normalization factor of the regularization function
δ^2	positive steering parameter
ζ	conjugate gradient update image
g	cost function gradient
g_{TV}	gradient of the total variation function
g_R	gradient of the regularization function
Ω	a bounded domain $\Omega \subset \Re^2$
N_Ω	area of the domain Ω

3.2. Noise model in US images

A relevant noise model for US image de-noising cannot be easily described. Generally, complex image formation process is considered. Recent research in the US image domain proves that multiplicative speckle noise distribution can be approximated by a Gamma distribution [46] or a Fisher–Tippett distribution [47]. Consequently, the general speckle noise model should be chosen as follows:

$$d(x,y) = f(x,y) + f(x,y)^m \cdot b(x,y) \quad (1)$$

$f(x,y)$ is the original image, $d(x,y)$ is the observed image, $b(x,y) \sim \aleph(0,\sigma^2)$ is a zero-mean Gaussian noise. This model

is more flexible and less restrictive than the usual radio-frequency model. It is able to capture reliably image statistics since the factor m depends on ultrasound devices and additional processing related to image formation. In opposition to additive white Gaussian noise model, the noise components in (1) are image-dependent. In [11] based on the experimental estimation of mean versus standard deviation in Log- Compressed images, Loupas et al. have shown that $m=0.5$ model fits better for data than the multiplicative model or Rayleigh model. Since, this model has been successfully used in many studies [11,43,44], in our approach, we use the TV formulation considering speckle noise model introduced by Loupas et al.

3.3. The proposed AWMTVR method

Inverse problems as image restoration consists of determining an approximation of original data $f(x,y)$ from a knowledge noisy image $d(x,y)$ on Ω.

In general this problem is both nonlinear and highly ill-posed. Uniqueness is in some ways a more interesting question, if the computed values of $f(x,y)$ are a solution to the inverse problem. In order to avoid the lack of rigorous results uniqueness, we propose to cast the inverse problem as an iterative optimization problem. Then a weighted total variation function is minimized as

$$J_{TV}(f,\Omega)=\frac{1}{N_\Omega}\cdot\int_\Omega W^2(f)|\nabla f|\,dx\,dy \tag{2}$$

where the squared weight W is used to facilitate the computations. The Weighted function is defined as follows:

$$W(f)=\frac{1}{\sqrt{|\nabla f|^2+\delta^2}} \tag{3}$$

Considering the model of Loupas et al. in (1), the total variation function J_{TV} is minimized taking into account a multiplicative regularization functional as the following:

$$J_R(d,f,\Omega)=\eta_R\int_\Omega\left(\frac{d-f}{f^m}\right)^2 dx\,dy \tag{4}$$

with

$$\eta_R=\frac{1}{\int_\Omega f^2 dx\,dy} \tag{5}$$

The minimization problem formulation is as follows:

Assume d the observed data and f an optimal solution to our problem, the cost function to be minimized is

$$J(d,f,\Omega)=J_{TV}(f,\Omega)\cdot J_R(d,f,\Omega) \tag{6}$$

3.3.1. Local minimum

Supposing that f satisfies the minimization problem of the non-quadratic cost functional J, the challenge is how to find its global minimum. Knowing that, the minimization problem may lead to several solutions in which the approximative solution to our problem exists, assuming the existence of a unique one. Therefore, the exact value is among obtained values and the global minimum is the one that satisfies these two conditions:

First, if J is defined in an interval $[a,b]$ with $a,b\in\Re$ and differentiable with respect to $\hat{f}$ where $\hat{f}\in[a,b]$ then $\nabla J(\hat{f})=0$,

Second, $\nabla^2 J(\hat{f})$ must to be positive on $\hat{f}$.

We assume that f_{approx} represents the approximative solution to our problem. Then, it can be written as a linear combination of an approximate solution and a generic direction ζ:

$$f=f_{approx}+\alpha\cdot\zeta \tag{7}$$

α being a real value. Substituting (7) into the cost functional (6) and considering the fact that the individual terms in the right-side of (6) vanish for the approximative solution, the minimization problem takes the form of

$$\hat{f}=\arg\min_{\alpha\ real}[J(d,(f_{approx}+\alpha\zeta),\Omega)] \tag{8}$$

Thus Eq. (8) can be written as follows:

$$\hat{f}=\arg\min_{\alpha\ real}\frac{(X\alpha^2+2Y\alpha+Z)(A\alpha^2-2B\alpha+C)}{(b\alpha+a)} \tag{9}$$

where

$$A=\eta_R\cdot\|\zeta^n\|_\Omega^2 \tag{10}$$

$$B=\eta_R\cdot real\langle d-f^{n-1},\zeta^n\rangle \tag{11}$$

$$C=\eta_R\cdot\|d-f^{n-1}\|_\Omega^2 \tag{12}$$

$$X=\eta_R\cdot\|W^{n-1}\cdot\nabla\zeta^n\|_\Omega^2 \tag{13}$$

$$Y=\eta_R\cdot real\langle W^{n-1}\cdot\nabla f^{n-1},W^{n-1}\cdot\nabla\zeta^n\rangle \tag{14}$$

$$Z=\eta_R\cdot\|W^{n-1}\cdot\nabla f^{n-1}\|_\Omega^2 \tag{15}$$

and

$$a=\eta_R\cdot\|(\zeta^n)^m\|_\Omega^2 \tag{16}$$

$$b=\eta_R\cdot\|(f^{n-1})^m\|_\Omega^2 \tag{17}$$

The norm over the bounded domain Ω is approximated by summing the vector magnitude $|\nabla f_{i,j}|$ over all pixels,

$$\|f\|_\Omega\approx\sum_{i=0}^{M-1}\sum_{j=0}^{N-1}|\nabla f_{i,j}|$$

where ∇f is the discrete gradient developed as follow:

In two dimensions, the discrete gradient of $f_{i,j}$, $(i,j)\in\mathbb{Z}^2$, is defined along the x and y dimensions as

$$\nabla f_{i,j}:=\begin{pmatrix}f_x(i,j)\\ f_y(i,j)\end{pmatrix}=\begin{pmatrix}\frac{\partial f_{i,j}}{\partial x}\\ \frac{\partial f_{i,j}}{\partial y}\end{pmatrix}.$$

where ∂ is the partial derivative, the Total Variation is defined as follows:

$$TV=\int_\Omega|\nabla f_{x,y}|\,dx\,dy$$

The inner product is computed as follows:

$$\langle d,f\rangle_\Omega=\int_\Omega d((x,y))\cdot\bar{f}((x,y))\,dx\,dy$$

where the over bar denotes complex conjugate.

3.3.2. Algorithm

Direct minimization of $J(d,f,\Omega)$ in (6) is unwanted because it leads to noisy data inversion. A Conjugate Gradient (CG) method is employed to optimize the problem, in which the cost functional $J(f,\Omega)$ changes as a function of iterations. Therefore, the algorithm involves an iterative sequence construction $\{f^n\}, n \geq 0$.

In the nth iteration, f^n update is found by minimizing the cost functional:

$$J^n(d,f^n,\Omega) = J^n_{TV}(f^n,\Omega)\cdot J^n_R(d,f^n,\Omega) \tag{18}$$

The regularization and the Total Variation functions are respectively given by

$$J^n_R(d,f^n,\Omega) = \frac{1}{\int_\Omega {f^n}^2\,dx\,dy}\cdot\int_\Omega\left(\frac{d-f^n}{(f^n)^m}\right)^2 dx\,dy \tag{19}$$

and

$$J^n_{TV}(f^n,\Omega) = \frac{1}{N_\Omega}\cdot\int_\Omega \frac{|\nabla f^n|}{|\nabla f^n|^2+\delta^2_n}\,dx\,dy \tag{20}$$

$N_\Omega = \int_\Omega dx\,dy$ denotes the area of the domain Ω.

In this work, the integral through Ω is calculated using the sum rule.

The proposed cost functional is based on the minimization of a weighted total variation factor and the observation that the minimization of the regularization function J_R converges to a constant factor. The cost functional form minimizes the total variation factor J_{TV} with a large cost because the weighting function values are still high. The regularization factor J^n_R will remain at a small value during the whole optimization process. Therefore the weight of the total variation factor will be more significant. And the noise will be at all times suppressed until optimization process stabilization.

The factor δ^2 in (3) is introduced for restoring differentiability to the TV-factor. We have chosen the value of δ^2 to be large in the beginning of the optimization. It will decrease gradually to small values to become constant at the end (Fig. 1). Thus, the optimization will restore the noisy image from the first iterations. In particular, δ^2 is chosen as follows:

$$\delta^2 = \frac{1}{|d-f^n|} \tag{21}$$

f^n represents an optimal solution to our problem.

We notice at the end that our algorithm belongs to an iterative regularization method. The proposed AWMTVR-filter updates the system solution as follows:

d is the observed image and f^n the approximative solution of the minimization problem. Then, we suppose that f^{n-1} is known. The sequence $\{f^n\}$ is constructed and updated as

$$f^0 = \overline{d}$$
$$f^n = f^{n-1}+\alpha^n\cdot\zeta^n,\quad n=1,2,3,\ldots \tag{22}$$

where α^n is a real parameter, ζ^n is a conjugate gradient update image and $\overline{d}$ is the mean image.

First, as the update for the image we take the gradient of J with respect to changes in the image f at the $(n-1)$ th iteration, i.e.,

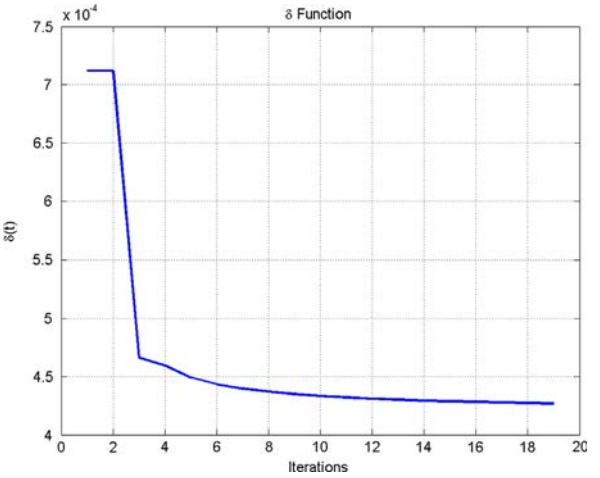

Fig. 1. δ function variations with respect to the iteration numbers.

$$\zeta^0 = g^0 = -\eta_M\cdot\frac{d^2-f_0^2}{f_0^2}$$
$$\zeta^n = g^n+\gamma^n_{PR}\cdot\zeta^{n-1},\quad n=1,2,3,\ldots \tag{23}$$

where ζ^0 is the gradient of the regularization function J^n_R with respect to f_0, γ^n_{PR} is the *Polak–Ribière* conjugate gradient directions, i.e.,

$$\gamma^n_{PR} = \frac{Real\langle g^n, g^n-g^{n-1}\rangle_\Omega}{\|g^{n-1}\|^2_\Omega} \tag{24}$$

and g^n is the gradient of the cost functional J^n with respect to f evaluated at the $(n-1)$ th iteration

$$g^n = g^n_{TV}\cdot J^{n-1}_R + J^{n-1}_{TV}\cdot g^n_R \tag{25}$$

In the optimization process, we start the procedure by using the mean image ($f^0=\overline{d}$) as the initial guess and by initializing the total variation factor at 1 ($J^0_{TV}=1$). In the reminder of the paper, m is included in the proposed filter as $m=0.5$.

Algorithm I.

1. Initialization: $\boldsymbol{f^0=\overline{d}, J^0_{TV}=1}$
2. Iteration: For $\boldsymbol{n=1,\ 2,\ 3,\ldots}$ Compute $\boldsymbol{f^{(n)}}$ by the following steps:
   (a) Compute $g^n = g^n_{TV}\cdot J^{n-1}_R + J^{n-1}_{TV}\cdot g^n_R$
   (b) Compute $\zeta^n = g^n+\gamma^n_{PR}\cdot\zeta^{n-1}\quad n=1,2,3,\ldots$
   (c) Compute α using the minimization problem
   $\hat{f} = \underset{\alpha\ real}{\boldsymbol{argmin}}[J(\boldsymbol{d},(\boldsymbol{f_{approx}}+\alpha\zeta),\Omega)]$
3. Compute $f^n = f^{n-1}+\alpha^n\cdot\zeta^n\quad n=1,2,3,\ldots$

If satisfies the stopping criteria
Stop iteration output;
else go to step 2(a)

3.4. The adaptive window mechanism

To maintain the image structure while reducing noise, windows with various sizes, shapes, and orientations are used [20]. Instead of using square windows, rectangular windows whose dimensions and orientations adapt to

local image details are used. Near a region boundary, the rectangular windows decrease and align with the boundary. In a homogeneous area, the windows will be enlarged which implies that the width l and height h of the window are related to the minimum and maximum differences between neighboring pixels and central one according to

$$l = \frac{a}{(l_n + 1)} \tag{26}$$

$$h = \frac{a}{(l_m + 1)} \tag{27}$$

Algorithm II.

1. **Input: a**: window size
2. **For** (i, j)=1, 2, …, (M, N) **Compute**:
   - $L = [L1,\ L2,\ L3,\ L4,\ L5]$
   - $l_n = |(\min(L))|$
   - $l_m = |(\max(L))|$
3. **Compute**: $l = \frac{a}{l_n + 1},\ h = \frac{a}{l_m + 1}$
4. Choose the appropriate window using the following tests:

If (L3 = = l_m) or (L2 = = l_m and L3 = = l_m and L4 = = l_m) or (L2 = = l_m and L3 = = l_m)
Then
Algorithm **I** is applied on a centered rectangular window to smooth the area around the treated pixel
Else If (L1 = = l_m) or (L5 = = l_m) or (L1 = = l_m and L2 = = l_m) or (L4 = = l_m and L5 = = l_m)
Then
Algorithm **I** is applied on a centered lying rectangular window to smooth the area around the treated pixel
Else If (L3 = = l_m and L4 = = l_m and L5 = = l_m) or (L4 = = l_m) or (L3 = = l_m and L5 = = l_m)
Then
Algorithm **I** is applied on a centered oblique window to smooth the area around the treated pixel
Else If (L1 = = l_m and L2 = = l_m and L3 = = l_m or (L2 = = l_m) or (L1 = = l_m and L3 = = l_m) **Then**
Algorithm **I** is applied on a centered oblique window to smooth the area around the treated pixel
Else Algorithm **I** is applied on a centered square window to smooth the area around the treated pixel **end**

where the addition of 1 in the denominator is to avoid division by zero. Parameter a is the proportionality term. l_n and l_m are the minimum and the maximum differences between neighboring pixels and central one, and are computed as in Fig. 2. More details on the used method are given in [20]. While traditional methods use a sliding window with fixed dimensions to smooth an image independently to the local content, in adaptive smoothing, the window size, shape and orientation are adapted to the local image context. Windows size is increased with decreasing neighboring distance magnitude and window shape and orientation are adjusted to smooth more in the direction of least neighboring pixel distances. In such a way, near a region boundary, the rectangular window becomes narrow and small and aligns with the boundary. In a homogeneous area, the window becomes square and large. The adaptive window contains fewer pixels when it is in a detailed area than in a homogeneous one, and pixels used in smoothing lie more along region boundaries than across them. Therefore, rather than performing smoothing noise isotropically, smoothing is performed in preferred orientations with optimal size and shape according to the local image structures (Fig. 3). This mechanism maintains edge details while reducing speckle noise within regions.

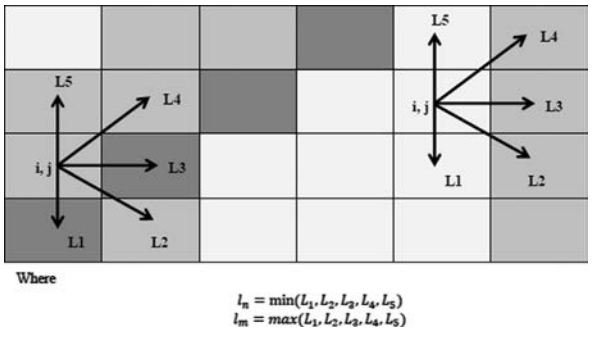

Fig. 2. The fifth directions computed around the pixel (i, j).

4. Experimental results

In this section, experimental results of the proposed method on both synthetic and ultrasound images are described. A comparative study with other speckle reduction methods is carried. The considered classical relevant filters are ATV (Additive Total Variation) [15], AD (Anisotropic Diffusion) [48] and Bilateral Filter [49]. All the experiments have been implemented on an i3 personal computer, 2.4 GHz, 4 GB RAM.

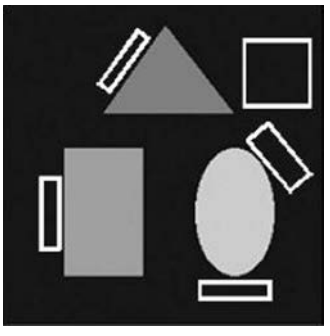

Fig. 3. Adaptive window (white windows) used in the proposed AWMTVR method.

4.1. Experiments on synthetic images

In order to evaluate and to measure the quality of the restoration, some quantitative measures are computed. FOM, PSNR, NMSE, MSSIM, FSIM and Q index are used to evaluate the capability of speckle reduction, edge preserving, feature similarity and image quality of the restored images. The computed evaluations are calculated only for simulated images for which original images are available for comparison.

4.1.1. Stopping criterion

The mean absolute error (MAE) between two adjacent steps can be used to stop the iteration:

$$MAE(f(n)) = \frac{1}{M \cdot N} \cdot \sum_{(i,j)=1}^{M,N} \sqrt{(f(i,j,n) - f(i,j,n-1))^2} \tag{28}$$

where $f(i,j,n)$ and $f(i,j,n-1)$ are the filtered values of the pixel (i,j) at time n and $n-1$, and M,N are respectively the numbers of columns and rows in the processed image.

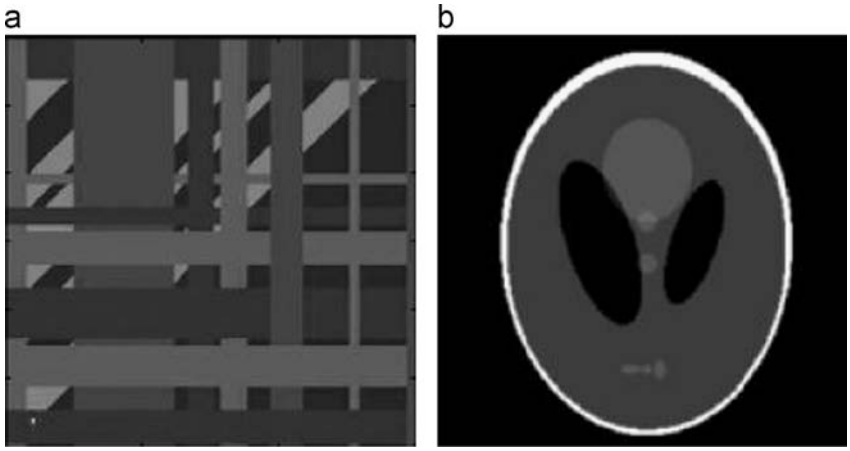

Fig. 4. Original images. (a) An image with intersected bars in different positions and directions, (b) a phantom image with different circular forms.

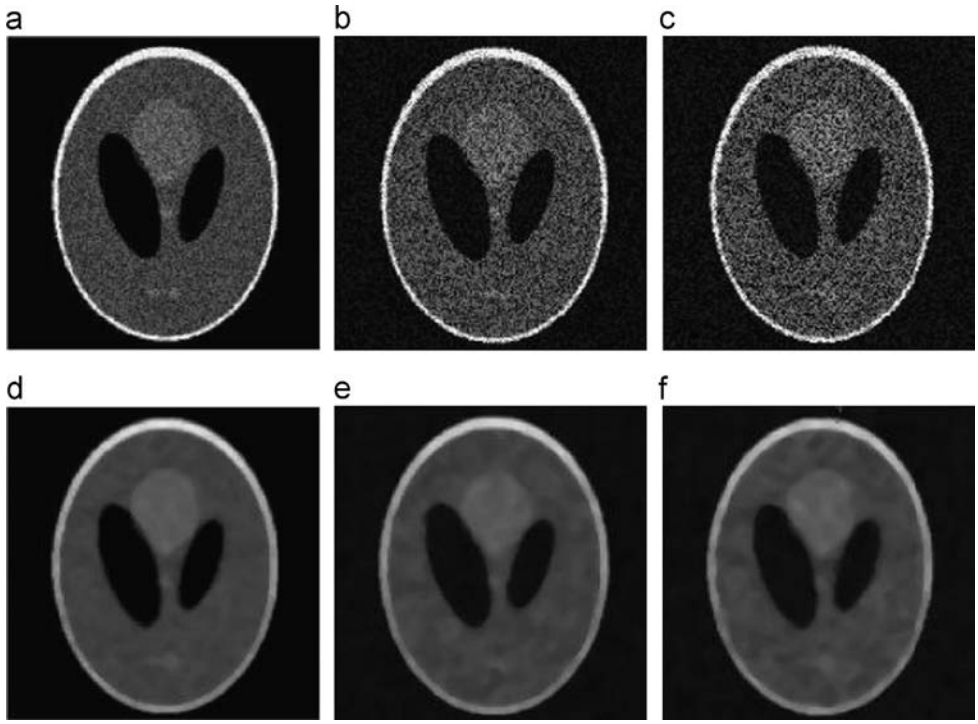

Fig. 5. Speckle removal capability of proposed algorithm with different speckle strength. (a, b, c) Synthetic noisy images using image model (1) with: $\sigma^2 = 2$, $\sigma^2 = 6$, $\sigma^2 = 10$; (d, e, f) corresponding images using method.

4.1.2. Performance evaluation

For a given observed image X and $\hat{X}$ its reconstructed image, performance evaluation tests, in terms of edge preservation, speckle reduction, feature similarity and image quality are defined as follows.

Edge preservation test: To compare the edge preservation performance of the different filtering approaches, Pratt's figure of merit is used. The figure of merit (FOM) is given by [50]

$$FOM = \frac{1}{\max\{\hat{N}, N_{ideal}\}} \cdot \sum_{(i,j)=1}^{\hat{N}} \frac{1}{1+d_i^2\beta} \tag{29}$$

where $\hat{N}$ and N_{ideal} are the number of detected and ideal edge pixels, d_i is the Euclidean distance between the ith detected edge pixel and the nearest ideal edge pixel and β is a constant typically set to $\frac{1}{9}$. FOM ranges between 0 and 1, with unity for the ideal edge detection.

Speckle reduction test: For each filtering operation, the measurement of ability to reduce the speckle noise is defined by the peak signal to noise ratio (PSNR) of the form:

$$PSNR = 20\log_{10}\left[\frac{2^n-1}{\sqrt{MSE}}\right] \text{ dB} \tag{30}$$

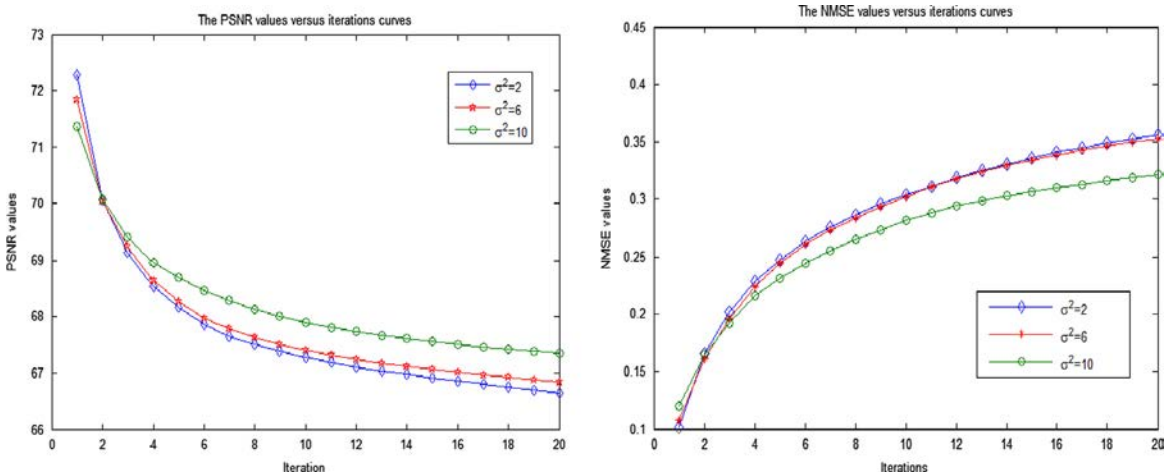

Fig. 6. PSNR and NMSE comparison for different speckle strength on phantom image (Fig. 4(b)) corrupted by speckle noise.

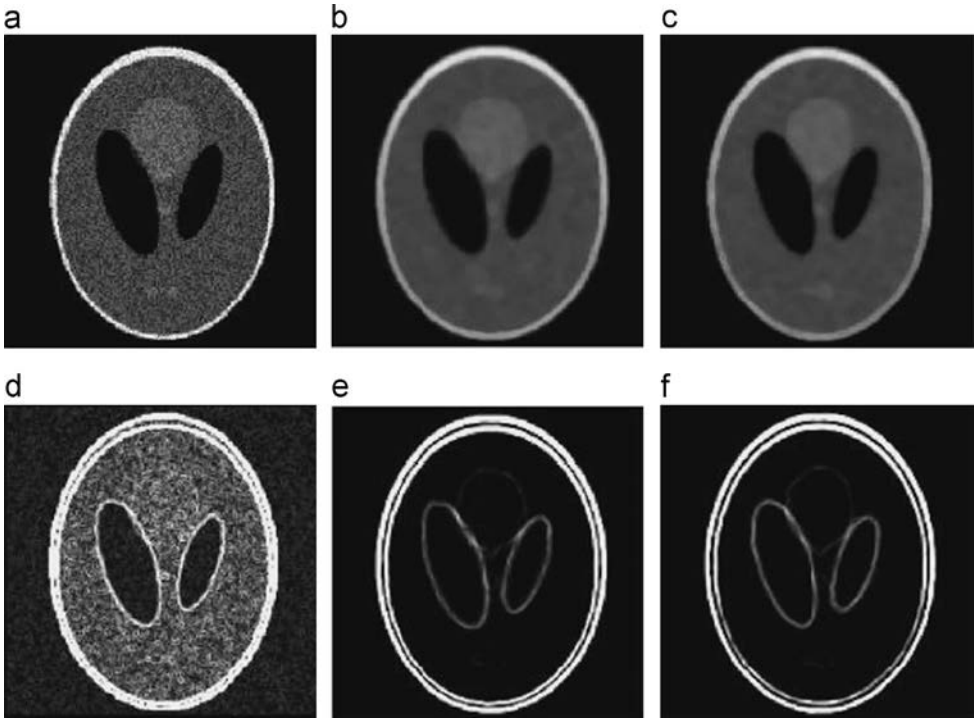

Fig. 7. (a) An image corrupted by speckle noise. (b) Traditional WMTVR filtering. (c) Adaptive WMTVR filtering. In the second row, (d, e, f) the gradient map of traditional and filtered images.

where n is the number of bits used in representing an image pixel. For grey scale image, n is 8. The mean-squared error (MSE) of the reconstructed image is defined as

$$MSE = \frac{\sum_{i=1}^{M}\sum_{j=1}^{N}|X(i,j)-\hat{X}(i,j)|^2}{M \times N} \tag{31}$$

where $X(i,j)$ is the original image, $\hat{X}(i,j)$ is the reconstructed image and the size of image is $M \times N$.

The normalized mean-squared error (NMSE) of the reconstructed image is defined as

$$NMSE = \frac{\sum_{i=1}^{M}\sum_{j=1}^{N}|X(i,j)-\hat{X}(i,j)|^2}{\sqrt{\sum_{i=1}^{M}\sum_{j=1}^{N}X(i,j)^2}\sqrt{\sum_{i=1}^{M}\sum_{j=1}^{N}\hat{X}(i,j)^2}} \tag{32}$$

where $X(i,j)$ is the original image and $\hat{X}(i,j)$ is the reconstructed image.

Structural similarity test: In order to evaluate the denoising filters, we propose to use the Mean SSIM (Mean Structural Similarity) index. This metric is based on a similarity measure between two images [51].

The MSSIM index is described as a function of three factors: the luminance, contrast and structural similarity. It is defined as

$$MSSIM\left(X,\hat{X}\right) = \frac{1}{M}\cdot\sum_{j=1}^{M} SSIM\left(x_j,y_j\right) \tag{33}$$

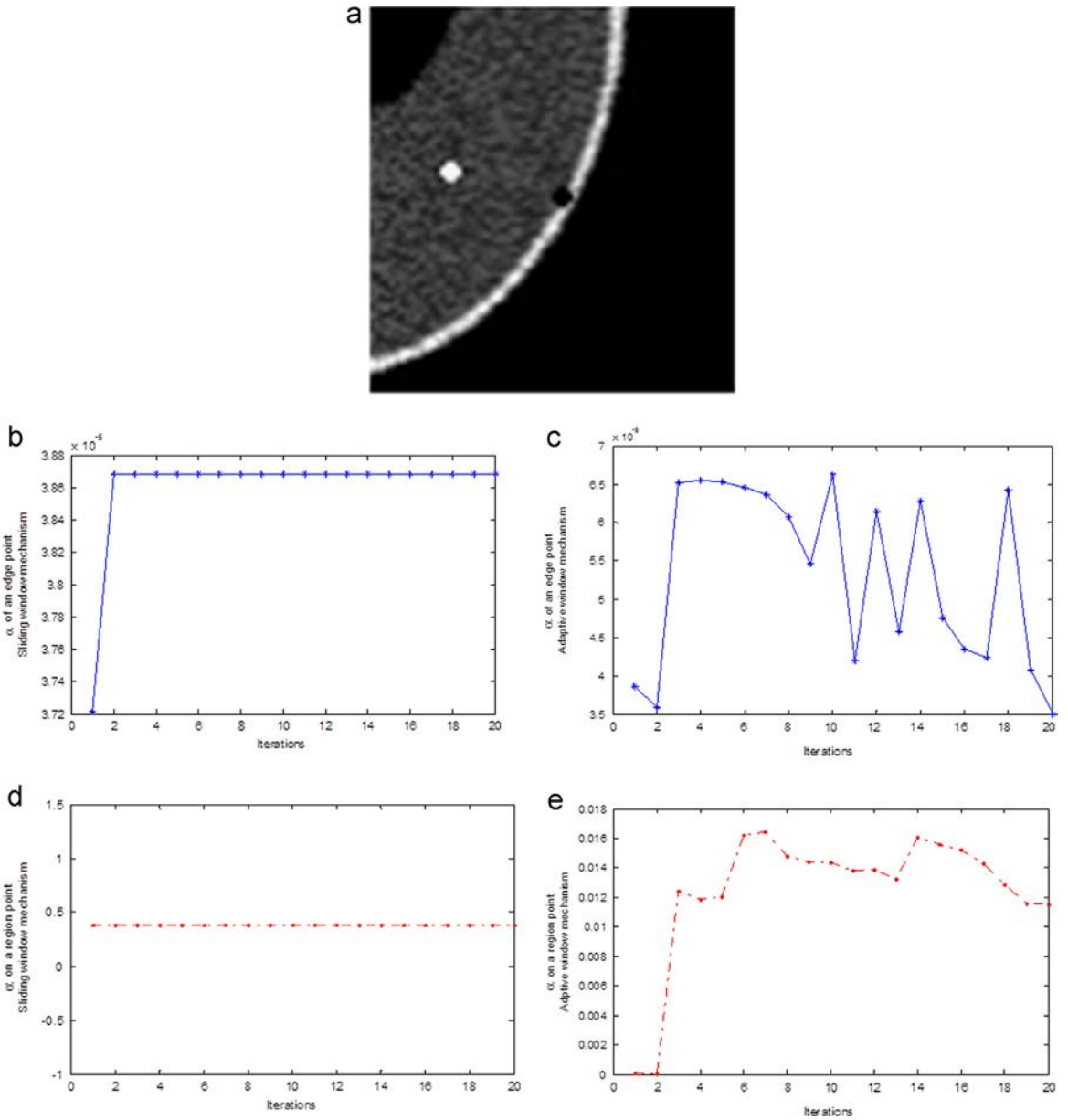

Fig. 8. Plots of the instantaneous parameter α as a function of iterations on the two critical points. (b) α using a sliding window (c) α using an adaptive window mechanism computed on an edge point (white point on (a)). (d) α using a sliding window (e) α using an adaptive window mechanism and computed on a region point (black point on (a)).

where X and $\hat{X}$ are respectively the original and the reconstructed images, x_j and y_j are the image contents at the jth local window and M is the number of windows. The *MSSIM* has values in [0,1], with unity representing structurally identical images.

The structural similarity (SSIM) is defined by

$$SSIM(x,y)=\frac{(2\mu_x\mu_y+C_1)(2\sigma_{xy}+C_2)}{(\mu_x^2+\mu_y^2+C_1)(\sigma_x^2+\sigma_y^2+C_2)} \tag{34}$$

where μ_x and μ_y are the mean intensity of x and y for luminance comparison, σ_x and σ_y are the standard deviation for contrast measurement and σ_{xy} is the correlation coefficient, $C_1=(K_1L)^2$, $C_2=(K_2L)^2$, where L is the dynamic range of the pixel intensities (255, for 8 bits Grey-scale images). $K_1 \ll 1$ and $K_2 \ll 1$ are small constant. For our experiments, we have used the following parameter settings: $K_1=0.001$ and $K_2=0.03$.

Feature similarity (FSIM) test: In [52] the authors have addressed the problem of the image quality assessment. An approach based on the fact that the human visual system (HVS) understands an image mainly according to its low-level feature is developed. Specifically, the phase congruency (*PC*), which is a dimensionless measure of the significance of a local structure, is used as the primary feature in FSIM. Considering that the *PC* is contrast invariant while the contrast information does affect the HVS perception of an image quality, the image gradient magnitude (*GM*) is employed as a secondary feature in FSIM. *PC* and *GM* play complementary roles in characterizing the image local quality.

At first, let PC_1 (PC_2) and GM_1 (GM_2) be the phase Congruency *PC* and the Gradient Magnitude *GM* of the image $X(\hat{X})$, respectively, the similarity between gray scale features is defined as

$$S_{PC}(x)=\frac{2PC_1(x)\cdot PC_2(x)+T_1}{PC_1^2(x)+PC_2^2(x)+T_1} \tag{35}$$

$$S_{GM}(x)=\frac{2GM_1(x)\cdot GM_2(x)+T_2}{GM_1^2(x)+GM_2^2(x)+T_2} \tag{36}$$

where T_1 and T_2 are positive constants. Since T_1 and T_2 components depend on the dynamic range of *PC* and *GM* values, in the experiments, both T_1 and T_2 will be fixed to all data. So that the proposed *FSIM* can be conveniently used. Then, $S_{PC}(x)$ and $S_{GM}(x)$ are combined to get the similarity $S_L(x)$ of X and $\hat{X}$, defined as

$$S_L=S_{PC}(x)\cdot S_{GM}(x) \tag{37}$$

where X and $\hat{X}$ are respectively the original and the reconstructed images. Finally, the *FSIM* index between X and $\hat{X}$ is defined as

$$FSIM=\frac{\sum_{x\in\Omega}S_L(x)\cdot PC(x)}{\sum_{x\in\Omega}PC(x)} \tag{38}$$

where Ω means the whole image spatial domain.

Image quality test: Let $X=\{X_i,\ i=1,2,\ldots,N\}$ and $\hat{X}=\{\hat{X}_i,\ i=1,2,\ldots,N\}$ be the reference image and the reconstructed image signals, respectively. The quality

Table 1
FOM, PSNR, NMSE, MSSIM, FSIM and Q values applied with several filters applied on two synthetic images.

	FOM	PSNR	NMSE	MSSIM	FSIM	Q
Image of Fig. 4(a)						
ATV	0.8405	**77.4514**	0.0415	0.8507	0.9659	0.3119
AD	0.7771	70.22	0.0614	0.7399	0.9762	0.3285
Bilateral	0.7707	77.2617	0.03029	0.7720	0.9697	0.3210
AWMTVR	**0.8618**	77.3159	**0.0168**	**0.8663**	**0.9929**	**0.6186**
Image of Fig. 4(b)						
ATV	0.9565	**75.0713**	0.334	0.7905	0.9850	0.4885
AD	0.8524	63.5433	0.2513	0.6336	0.9891	0.4788
Bilateral	0.6119	74.5079	0.1595	0.8135	0.9811	0.4224
AWMTVR	**0.9599**	74.2363	**0.1141**	**0.9177**	**0.9892**	**0.4903**

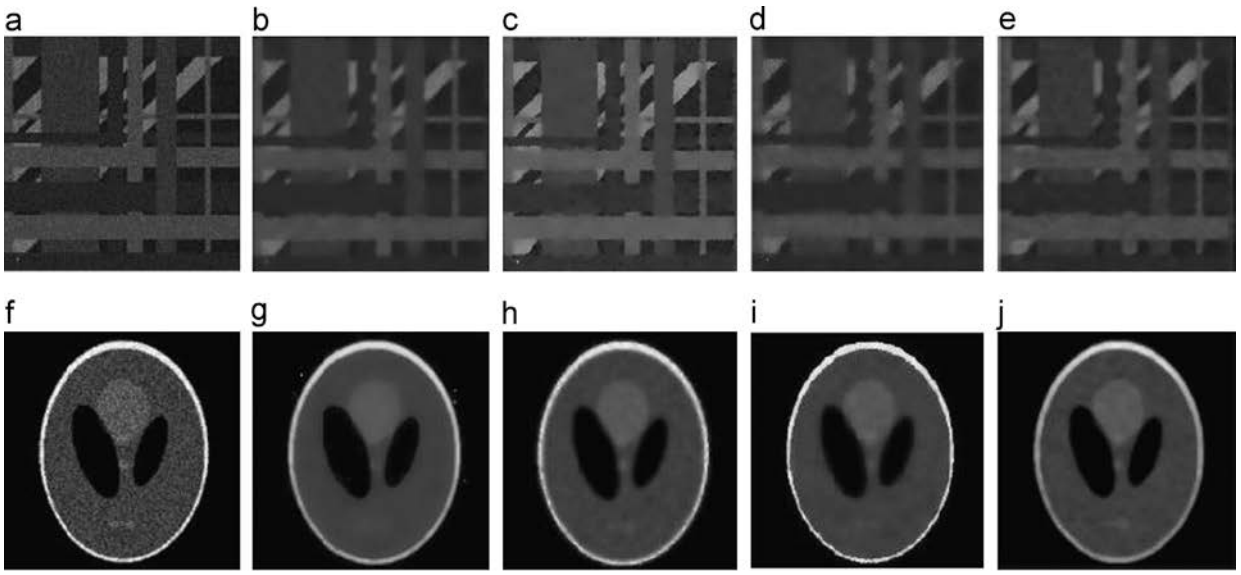

Fig. 9. Comparison of different speckle reduction methods. (a, f) Synthetic noisy images using model (1) with $\sigma^2=2$; (b, g) restored image by ATV model; (c, h) restored image by AD model; (d, i) restored image by Bilateral method; (e, j) restored image by proposed method.

index Q is defined as [53]

$$Q = \frac{4\sigma_{X\hat{X}}\overline{X}\overline{\hat{X}}}{(\sigma_X^2+\sigma_{\hat{X}}^2)[(\overline{X})^2+(\overline{\hat{X}})^2]} \tag{39}$$

where

$$\overline{X} = \frac{1}{N}\sum_{i=1}^{N} X_i, \quad \overline{\hat{X}} = \frac{1}{N}\sum_{i=1}^{N} \hat{X}_i,$$

$$\sigma_X^2 = \frac{1}{N-1}\sum_{i=1}^{N} (X_i-\overline{X})^2$$

$$\sigma_{\hat{X}}^2 = \frac{1}{N-1}\sum_{i=1}^{N} (\hat{X}_i-\overline{\hat{X}})^2$$

$$\sigma_{X\hat{X}} = \frac{1}{N-1}\sum_{i=1}^{N} (X_i-\overline{X})\left(\hat{X}_i-\overline{\hat{X}}\right)$$

The dynamic range of Q is $[-1, 1]$. The best value 1 is achieved if and only if $\hat{X}_i = X_i$ for all $i = 1, 2, \ldots, N$. The lowest value of -1 occurs when $\hat{X}_i = 2\overline{X} - X_i$ for all $i = 1, 2, \ldots, N$. This quality index models any distortion as a combination of three different factors: loss of correlation, luminance distortion, and contrast distortion. The quality measurement is applied to local regions using a sliding window approach. The local quality index Q_j is computed within the sliding window. If there are a total of M windows, the overall quality index is given by

$$\hat{Q} = \frac{1}{M}\sum_{j=1}^{M} Q_j \tag{40}$$

Table 2
Elapsed time for the four methods.

177 × 175 (pixels)	**Iterations**	**Execution time (s)**
Phantom image		
ATV	20	3.33
AD	20	1.977
Bilateral	1	3.056
AWMTVR	4	4.31
180 × 171 (pixels)	**Iterations**	**Execution time (s)**
Bar image		
ATV	20	2.97
AD	20	2.392
Bilateral	1	2.959
AWMTVR	4	5.919

4.2. Results and comparison

The suggested method has been tested on original images of Fig. 4(a) and (b) corrupted by a speckle noise with standard deviation $\sigma^2 = 2$, $\sigma^2 = 6$ and $\sigma^2 = 10$. De-noising these images using our algorithm has been performed respectively in 4, 7 and 10 iterations for noise with standard deviations values cited above. The images of Fig. 5 illustrate the results of AWMTVR filter on synthetic images. It is observed that the more an image is noisy, the less is the noise reduction. Even the image is quite noisy, the proposed

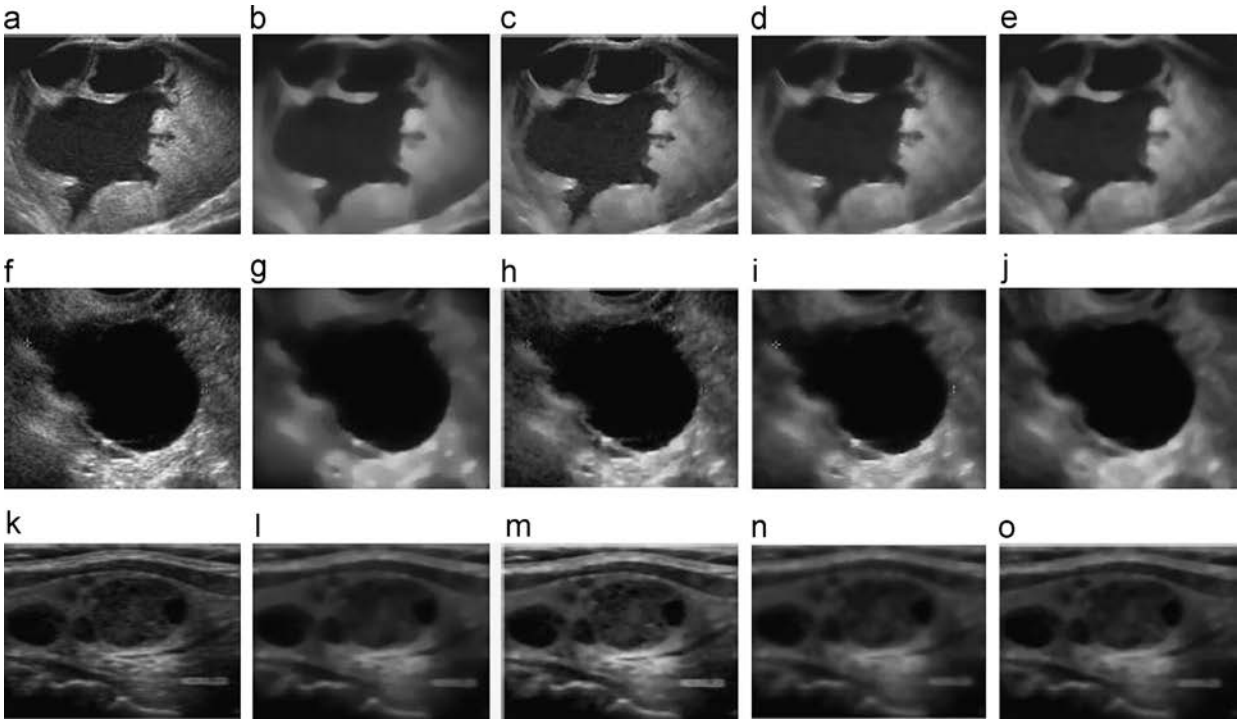

Fig. 10. Comparison with different methods on ultrasound images. (a) A real ultrasound ovary cancer image; (f) a real breast cancer mass ultrasound image; (k) a real ultrasound thyroid nodules image; (b, g, l) restored images by ATV model; (c, h, m) restored images by AD model; (d, i, n) restored images by Bilateral method; (e, j, o) restored images by proposed method.

method can improve the image quality. The plots of the PSNR and NMSE show a decreasing respectively an increasing of their values versus the number of iterations and the noise strength. The PSNR (NMSE) values decrease (increase) versus the number of iterations because in the first iteration the noise is at its maximum values so the de-noising is maximum, i.e. when PSNR takes great values, the noise is reduced, and consequently the PSNR is decreased and when NMSE takes low values, the noise is reduced, and consequently the NMSE is increased. The effectiveness of the method is clearly shown in Fig. 6.

In order to demonstrate the importance of the adaptive window mechanism in maintaining edge details while reducing speckle noise within regions, we propose in this section to compare the sliding and the adaptive mechanisms. Fig. 7 illustrates a comparison of the Adaptive WMTVR speckle reduction method with the WMTVR method applied to a synthetic phantom image. At a glance,

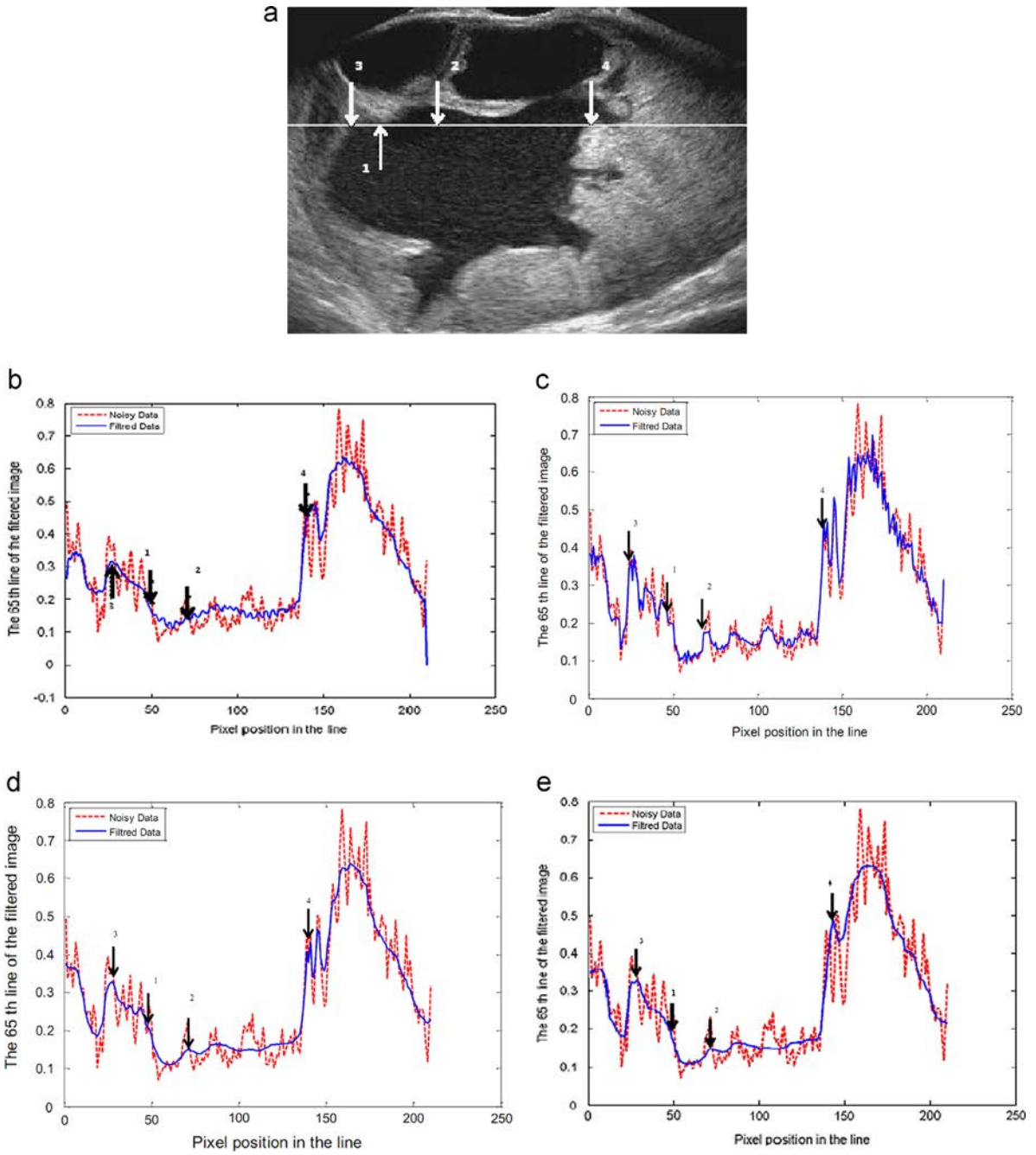

Fig. 11. Corresponding signal of one row, (a) with row 65; (b) restored image by ATV model; (c) restored image by AD model; (d) restored image by Bilateral method; (e) restored image by proposed method.

images of Fig. 7(c) and (f) look alike but when examined more closely it is clear that small details are preserved by the adaptive method better than the sliding method.

The local variation of the parameter α over 20 iterations on two critical points has been computed, one of them is situated on an edge named *edge point* and the other one is situated on a region area called *region point*, as illustrated in Fig. 8(a). Using the adaptive window mechanism, α is instantaneously computed. For each iteration α values are small on or near an edge and large on a homogeneous area. When using a sliding window, α is always the same and does not adapt to each iteration. While using adaptive window method, α is computed with more accuracy than a fixed window method. We conclude that the adaptive window mechanism adapts to each image detail which favors a better image structures preservation than the classical one.

Table 1 summarizes FOM, PSNR, NMSE, MSSIM, FSIM and Q for the synthetic images. Table values corroborate the visual observation. In these evaluation frameworks, the ATV model has a large PSNR value than the other models in most tests. Therefore, it reduces only noise.

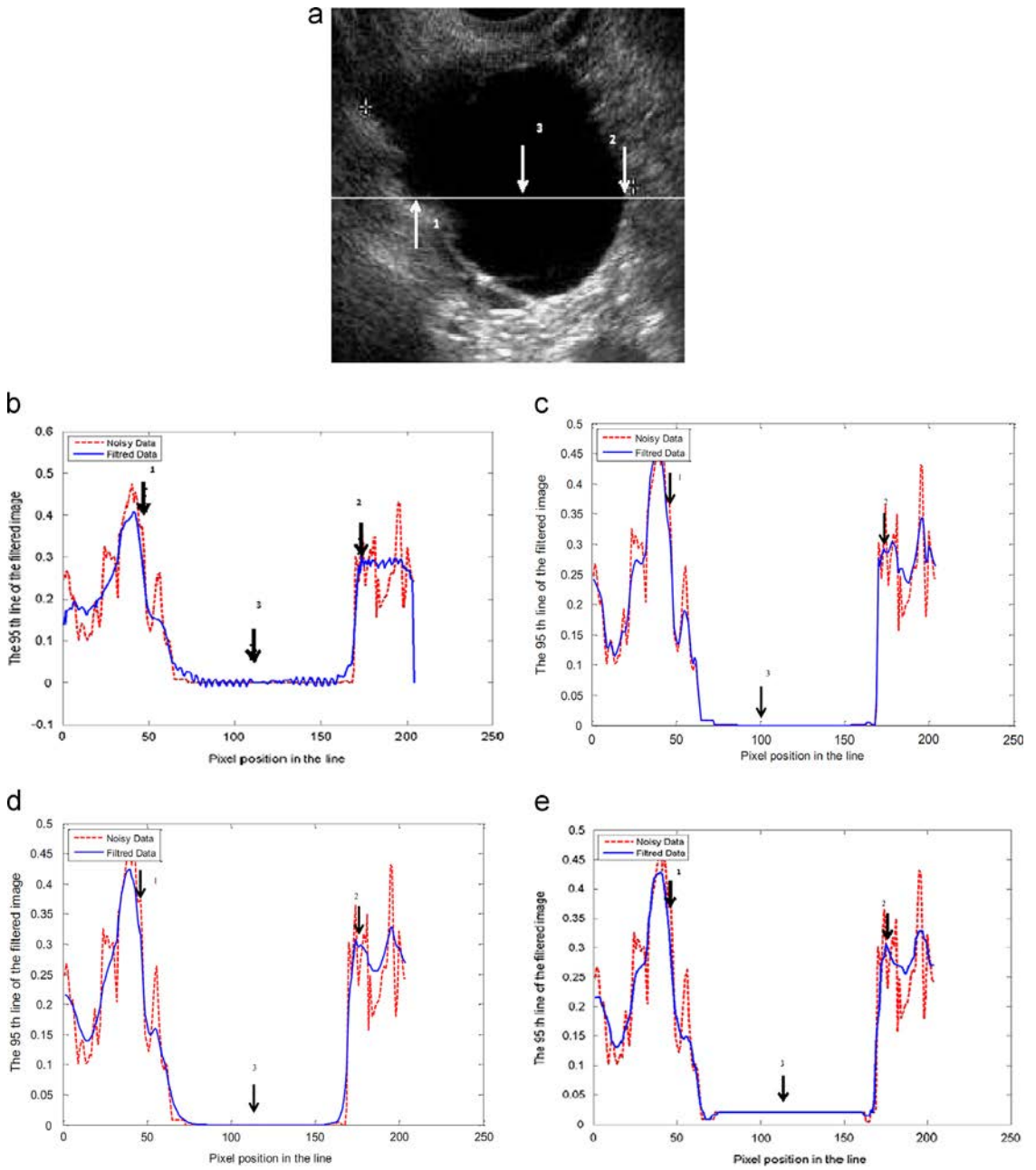

Fig. 12. Corresponding signal of one row, (a) with row 95; (b) restored image by ATV model; (c) restored image by AD model; (d) restored image by Bilateral method; (e) restored image by proposed method.

For all tests, the FOM and MSSIM values for the ATV model are slightly higher than Bilateral and AD filters which indicate less similarity between the original and the filtered images and less edge preservation for the two models. Yet, FSIM and Quality index of the AD model are higher than Bilateral and ATV models which reveal that AD model outperforms the two models in terms of image quality and feature similarity. However, the proposed AWMTVR algorithm produces the highest FOM, NMSE, MSSIM, FSIM and Q index values, with large PSNR which means that the proposed method has been able to reduce the noise significantly without blurring or changing the image features and structures more than the other tested models.

Based on these tests, the AWMTVR retains more structures in the de-noised images than the other three methods. It can suppress the noise well, while keeping edges and fine details. In Fig. 9, we compare visually our model with other three popular speckle removal methods. The simulated noisy images are constructed based on

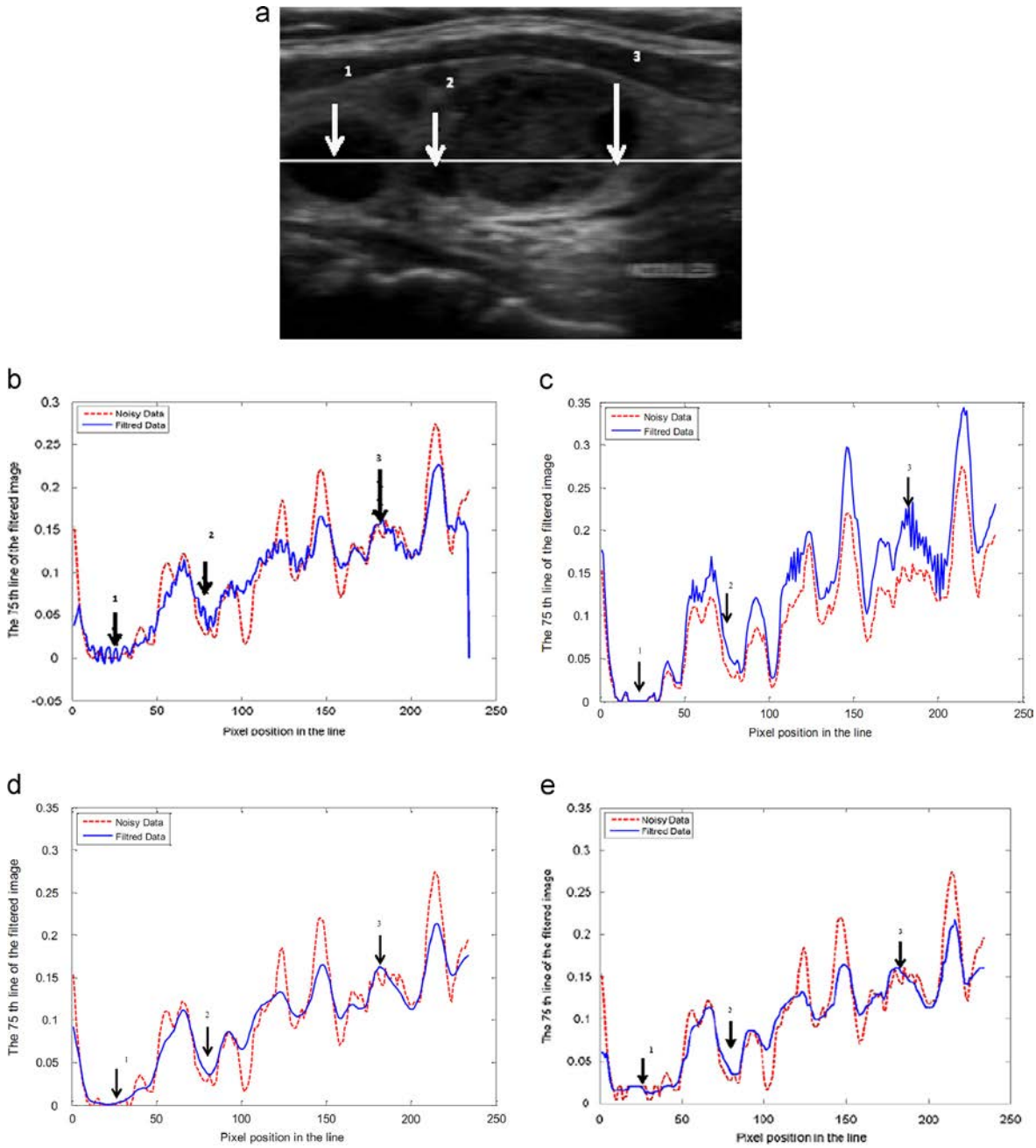

Fig. 13. Corresponding signal of one row, (a) with row 75; (b) restored image by ATV model; (c) restored image by AD model; (d) restored image by Bilateral method; (e) restored image by proposed method.

Eq. (1) with $\sigma^2 = 2$ (Fig. 9(a, f)). In the experiments, the AD filter removes noise but blurs the image edges and the linear targets (Fig. 9(c, h)), the Bilateral de-speckles well but some noise appears in the object boundaries (Fig. 9(d, i)). The ATV method can remove speckle noise and retain edges (Fig. 9(b, g)). Nevertheless, some artifacts appear in the homogeneous region. The proposed method is the most effective for removing noise, keeping image features and edges with the higher values for all the quality metrics. Although, it is slower than ATV, AD and Bilateral methods, for an image of size 177×175 pixels, the proposed method takes 4.301 s, and for an image of size 180×171 pixels, it takes 5.919 s. The corresponding tests are reported in Table 2. The results correspond to the number of iterations for all tested methods and the execution time against the number of iterations. AWMTVR execution time is a bit higher compared to the other methods because of its adaptive property. For one iteration, Algorithm II (Adaptive windows) calls 30 975 times Algorithm I (WMTVR) for an image of size 177×175 and 30 780 times for an image sized 180×171. However, our filter reduces the number of iterations while yielding good results. Using adaptive windows provides to the multiplicative regularization a local processing which improves the restoration results and makes the proposed algorithm good and competitive with the existing methods.

4.3. Experiments on real US images

In this section, we test the performance of the proposed method on real ultrasound images and compare with three other methods. Fig. 10 shows the results on three real ultrasound images used in our experiments. From this figure, we can see the experiments on the real ultrasound abdomen image, the breast cancer mass image and the thyroid nodules image. It is noticed that the restored images using AD model mix a boundary of the mass region with the background region (Fig. 10(c, h, m)). It causes loss of information regarding the important details of the image. ATV method gives good results however strong artifacts have been observed (Fig. 10(b, g, l)). Bilateral (Fig. 10(d, i, n)) and proposed method (Fig. 10(e, j, o)) have a better performance than the other two methods. Figs. 11–13 show the pixel values on one row of the image (the highlighted line) versus the column positions. From figures, labels 1–4 are marked a corresponding region or transition. From Fig. 11(a) labels 1 and 2 indicate the limit of the ovary mass, labels 3 and 4 are the limits of the outer region. In Fig. 12(a), labels 1 and 2 limit the solid breast cancer, label 3 the interior solid region. In Fig. 13(a), labels illustrate 3 thyroid nodules. Filtering operation along the marked row shows the potential transitions and smoothed areas and reveals the effectiveness of the tested methods.

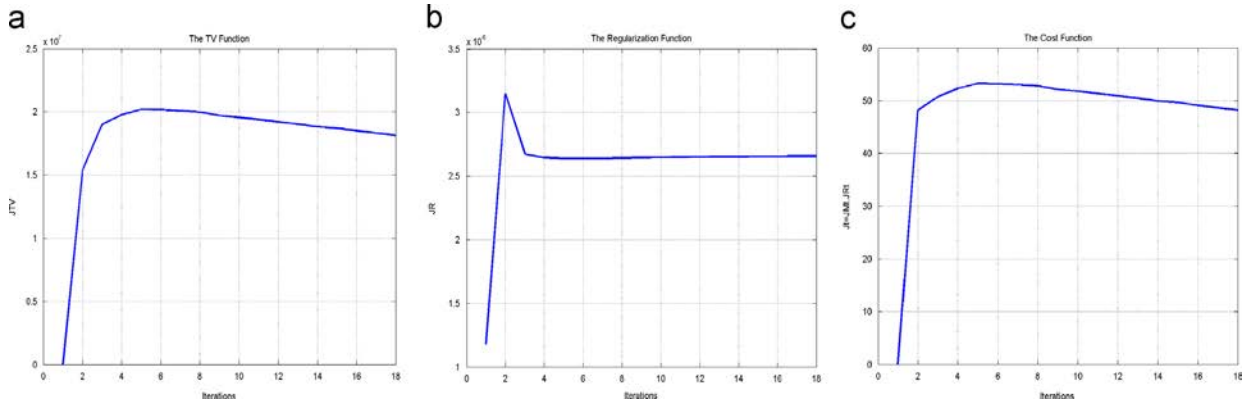

Fig. 14. Minimization versus to the number of iterations. (a) J_{TV} function. (b) J_R function. (c) Cost function $J = J_{TV} \cdot J_R$.

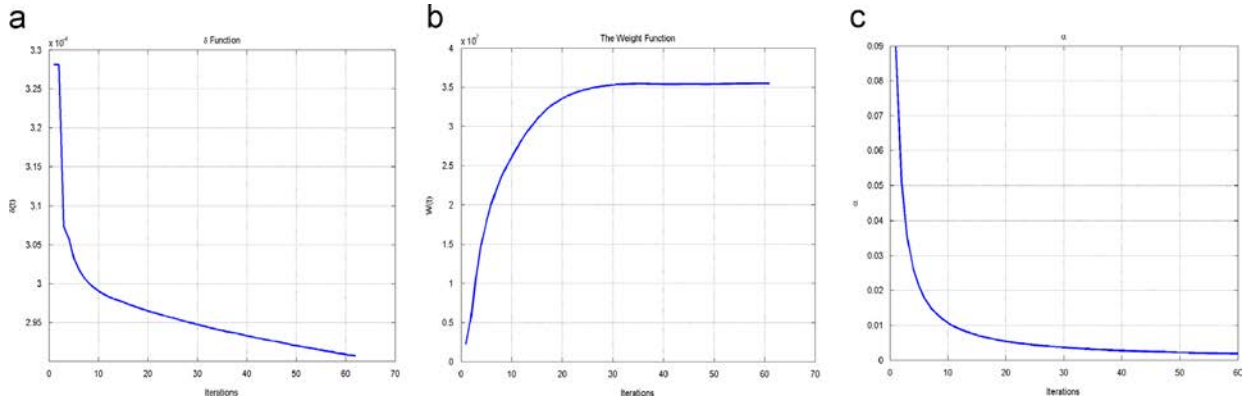

Fig. 15. Test functions versus the number of iterations. (a) Factor δ^n. (b) Weight function W^n. (c) Global minimum α^n.

ATV presents some artifacts (Figs. 11–13(b)). AD, Bilateral and the proposed method operate better than ATV. However some fine details are over smoothed using AD and Bilateral filters.

Finally, Fig. 14(a) presents the TV functional J_{TV}, the J_R and J as functions of the iteration's number n. We observe that J_{TV} converges slower than the Regularization function J_R (Fig. 14(b)). The Cost functional J is represented in Fig. 14 (c). Fig. 15(a–c) exhibits the quantity δ^n, the weight function W^n and the parameter α^n which is computed as the mean of local $\alpha_{i,j}^n$ through each iteration. Considering these parameters, it is assumed that our algorithm converges in few iterations.

5. Conclusion

A new adaptive filter approach, Adaptive Weighted Multiplicative Total Variation regularization (AWMTVR), is proposed for suppressing speckle while preserving texture feature in US medical images. The filter is based on an adaptation of a multiplicative regularization function. The new functional combines a data misfit function based on Loupas et al. model and a Weighted Total Variation (WTV) function as a multiplicative factor in the cost functional. The basic goal of the multiplicative form is to eliminate the choice of the artificial regularization parameter. The proposed method uses the conjugate gradient algorithm to update the approximative solution of the minimization problem. The filtering process of the AWMTVR is performed on an adaptive window with various shapes, sizes and orientations. This adaptive window method calculates the instantaneous coefficient of variation for the edge area with more accuracy than a fixed window. We have compared the proposed method with three other popular speckle reduction methods in terms of image quality, speckle reduction, edge and feature preservation performance. Our method is effective to remove speckle noise and has competitive results on synthetic images as well as on real US images.

Acknowledgments

The authors would like to thank the anonymous reviewers, whose valuable comments and suggestions have helped to considerably improve the quality of the paper.

References

[1] A. Webb, Introduction to Biomedical Imaging, John Wiley and Sons, Hoboken, 2003.
[2] J.W. Goodman, Some fundamental properties of speckle, J. Opt. Soc. Am. 66 (11) (1976) 1145–1150.
[3] J.W. Goodman, Laser speckle and related phenomena, in: J.-C. Dainty (Ed.), Statistical Properties of Laser Speckle Patterns, Springer, New York, 1985.
[4] C. Oliver, S. Quegan, Understanding Synthetic Aperture Radar Images, vol. 31(4), Artech House, 1998.
[5] D. Kaplan, Q. Ma, On the statistical characteristics of the log-compressed Rayleigh signals: theoretical formulation and experimental results, J. Acoust. Soc. Am. 95 (1994) 1396–1400.
[6] R.F. Wagner, M. Insana, S. Smith, Fundamental correlation lengths of coherent speckle in medical ultrasonic images, IEEE Trans. Ultrason. Ferroelectr. Freq. Control 35 (1988) 34–44.
[7] M.F. Insanna, R.F. Wagner, B.S. Garra, D.G. Brown, T.H. Shawker, Analysis of ultrasound image texture via generalized Rician statistics, Opt. Eng. 25 (1986) 743–748.
[8] V. Dutt, J.F. Greenleaf, Adaptive speckle reduction filter for log-compressed B-scan images, IEEE Trans. Med. Imaging 15 (1996) 802–813.
[9] J. Goodman, Laser Speckle and Related Phenomena, Springer-Verlag, Berlin, 1984, pp. 7–95.
[10] J.M. Thijssen, B. Oosterveld, Speckle and texture in echography artifact or information, in: IEEE Transaction on Ultrasonics Symposium Proceedings, vol. 2, 2003, pp. 803–810.
[11] A. Loupas, Digital image processing for noise reduction in medical ultra sons (Ph.D. thesis), University of Edinburgh, UK, 1998.
[12] G. Aubert, J. Aujol, A variational approach to remove multiplicative noise, SIAM J. Appl. Math. 68 (4) (2008) 925–946.
[13] Y. Huang, M. Ng, Y. Wen, A new total variation method for multiplicative noise removal, SIAM J. Imaging Sci. 2 (1) (2009) 20–40.
[14] L. Rudin, P. Lions, S. Osher, Multiplicative de-noising and deblurring: theory and algorithms, in: S. Osher, N. Paragios (Eds.), Geometric Level Set Methods in Imaging, Vision, and Graphics, 2003, pp. 103–120.
[15] J. Shi, S. Osher, A Nonlinear Inverse Scale Space Method for a Convex Multiplicative Noise Model, Technical Report 07-10, Computational and Applied Math, University of California, Los Angeles, 2007.
[16] K. Djemal, Speckle reduction in ultrasound images by minimization of total variation, in: IEEE International Conference on Image Processing, ICIP, 2005.
[17] P.M. van den Berg, A.L. van Brockhoven, A. Abubakar, Extended contrast source inversion, Inverse Probl. 15 (1999) 1325–1344.
[18] G. Liu, X. Zeng, F. Tian, Z. Li, K. Chaiboul, An adaptive total variation method for speckle reduction in medical ultrasound imaging, Signal Process. 89 (2009) 2233–2243.
[19] J.S. Lee, Digital image enhancement and noise filtering by use of local statistics, IEEE Trans. Pattern Anal. Mach. Intell. 2 (2) (1980) 165–168.
[20] D.T. Kuan, A.A. Sawchuck, T.C. Strand, P. Chavel, Adaptive noise smoothing filter for images with signal dependent noise, IEEE Trans. Pattern Anal. Mach. Intell. 7 (2) (1985) 165–177.
[21] V.S. Frost, J.A. Stiles, K.S. Shanmugan, J.C. Holtzman, A model for radar images and its application to adaptive digital filtering of multiplicative noise, IEEE Trans. Pattern Anal. Mach. Intell. 4 (2) (1982) 157–166.
[22] A. Lopes, R. Touzi, E. Nezry, Adaptive speckle filters and scene heterogeneity, IEEE Trans. Geosci. Remote Sens. 28 (6) (1990) 92–1000.
[23] M. Bertero, P. Boccacci, Introduction to Inverse Problems in Imaging, IOP Publishing, Bristol, UK, 1998.
[24] P.J. Hauber, Robust Statistics, Wiley, New York, 2003.
[25] L. Rudin, S. Osher, E. Fatemi, Nonlinear total variation based noise removal algorithm, Physica D 60 (1992) 259–268.
[26] A. Ogier, P. Hellier, C. Barillotl, Speckle reduction on ultrasound images by variational methods and adaptive Lagrangian multipliers, in: IEEE International Symposium on Biomedical Imaging: Nano to Macro, vol. 1, 2004, pp. 547–550.
[27] Banazier A. Abrahim, Yasser Kadah, Speckle noise reduction method combining total variation and wavelet shrinkage for clinical ultrasound imaging, in: IEEE International Conference on Image Processing, ICIP, 2011, pp. 80–83.
[28] Fangfang Dong, Zhen Liu, Jialin Peng, A novel variational model for multiplicative noise removal by combining nonlocal and weberized total variation regularization, in: 4th International Congress on Image and Signal Processing (CISP), vol. 1, 2011, pp. 42–46.
[29] Y. Shi, R. Molina, X. Yang, New total variation regularized L1 model for image restoration, Digital Signal Process. 20 (2010) 1656–1676.
[30] Y. Hao, X. Feng, J. Xu, Multiplicative noise removal via sparse and redundant representation over learned dictionnaries and total variation, Signal Process. 92 (2012) 1536–1549.
[31] A. Gholami, S.M. Hosseini, A balanced combination of Tikhonov and total variation regularizations for reconstruction of piecewise-smooth signals, Signal Process. 93 (2013) 1945–1960.
[32] L. Wang, L. Xiao, J. Zhangi, Z. Wei, New image restoration method associated with tetrolets shrinkage and weighted anisotropic total variation, Signal Process. 93 (2013) 661–670.
[33] S.D. Babacan, R. Molina, A.K. Katsaggelos, Parameter estimation in TV image restoration using variational distribution approximation, IEEE Trans. Image Process. 17 (March (3)) (2008) 326–339.
[34] M. Bertalmio, V. Caselles, B. Rougé, A. Solé, TV based image restoration with local constraints, IEEE Trans. J. Sci. Comput. 19 (2003) 95–122.

[35] J. Bioucas-Dias, M. Figueiredo, J. Oliveira, Adaptive Bayesian/total-variation image deconvolution: a majorization–minimization approach, in: EUSIPCO′ 2006, 2006.
[36] J. Bioucas-Dias, M. Figueiredo, J. Oliveira, Total-variation image deconvolution: a majorization–minimization approach, in: ICASSP′2006, 2006.
[37] S. Derin Babacan, R. Molina, A.K. Katsaggelos, Total variation image restoration and parameter estimation using variational posterior distribution approximation, in: ICIP′2007, 2007, pp. 97–100.
[38] Y.Z. Lin, B. Wohlberg, H. Guo, UPRE method for total variation parameter selection, Signal Process. 90 (2010) 2546–2551.
[39] A. Abubakar, P.M. van den Berg, J.T. Fokkema, Towards non-linear inversion for characterization of time-lapse phenomena through numerical modellings, Geophys. Prospect. 51 (2003) 285–293.
[40] A. Abubakar, P.M. van den Berg, T.M. Habashy, Application of the multiplicative regularized contrast source inversion method on TM- and TE-polarized experimental Fresnal data inverse problems, IOP Sci. Inverse Probl. 21S (2005) S5–S13.
[41] A. Abubakar, T.M. Habashy, P.M. van den Berg, Nonlinear inversion of multi-frequency microwave Fresnel Data using Multiplicative Regularized contrast source inversion, Prog. Electromagn. Res. 62 (2006) 193–201.
[42] S.Y. Semenov, A.E. Bulyshev, A. Abubakar, et al., Microwave-tomographic imaging of the high-dielectric-contrast objects using different image-reconstruction approaches, IEEE Trans. Microw. Theory Tech. 53 (2005) 2284–2294.
[43] A. Abubakar, P.M. van den Berg, S.Y. Semenov, Two- and three-dimensional algorithms for microwave imaging and inverse scattering, J. Electromagn. Waves Appl. 17 (2) (2003) 209–231.
[44] T.M. Habashy, A. Abubakar, A general framework for constraint minimization for the inversion of electromagnetic measurements, Prog. Electromagn. Res. 46 (2004) 265–312.
[45] P.M. van den Berg, A. Abubakar, J.T. Fokkema, Multiplicative regularization for contrast profile inversion, Radio Sci. 38 (2) (2003). 23 (1–10).
[46] Z. Tao, H.D. Tagare, J.D. Beaty, Evaluation of four probability distribution models for speckle in clinical cardiac ultrasound images, IEEE Trans. Med. Imaging 25 (2006) 1483–1491.
[47] G.S. Slabaugh, G. Unal, T. Fang, M. Wels, Ultrasound-specific segmentation via de correlation and statistical region-based active contours, in: Proceedings of IEEE Computer Society Conference on Computer Vision and Pattern Recognition, vol. 1, 2006, pp. 45–53.
[48] S. Aja Fernandez, C. Alberola Lopez, On the estimation of the coefficient of variation for anisotropic diffusion speckle filtering, IEEE Trans. Image Process. 15 (September (9)) (2006) 2694–2701.
[49] E. Farzana, M. Tanzid, K.M. Mohsin, M.I.H. Bhuiyan, S. Hossain, Adaptive bilateral filtering for despeckling of medical ultrasound images, in: TENCON 2010 – 2010 IEEE Region 10 Conference, 2010, pp. 1728–1733.
[50] W.K. Pratt, Digital Image Processing, Wiley, New York, 1977.
[51] Z. Wang, A.C. Bovik, H.R. Sheikh, E.P. Simoncelli, Image quality assessment: from error visibility to structural similarity, IEEE Trans. Image Process. 14 (3) (2004) 600–612.
[52] L. Zhang, L. Zhang, X. Mou, D. Zhang, FSIM: a feature similarity index for image quality assessment, IEEE Trans. Image Process. 20 (8) (2011) 2378–2386.
[53] Z. Wang, Alan C. Bovik, A universal image quality index, IEEE Signal Process. Lett. 9 (March (3)) (2002).